Biochimica et Biophysica Acta 1850 (2015) 141–149

Contents lists available at ScienceDirect

Biochimica et Biophysica Acta

journal homepage: www.elsevier.com/locate/bbagen

Bridging of a substrate between cyclodextrin and an enzyme's active site pocket triggers a unique mode of inhibition ☆

Nitesh V. Sule [a,*], Angel Ugrinov [a], Sanku Mallik [b], D.K. Srivastava [a,**]

[a] Department of Chemistry & Biochemistry, North Dakota State University, Fargo, ND 58108, United States
[b] Pharmaceutical Sciences, North Dakota State University, Fargo, ND 58108, United States

ARTICLE INFO

Article history:
Received 8 September 2014
Received in revised form 14 October 2014
Accepted 17 October 2014
Available online 24 October 2014

Keywords:
Substrate bridging
Cyclodextrin
Methionine aminopeptidase
Inhibition
Cyclodextrin–substrate complex
Molecular modeling

ABSTRACT

Background: Methionyl-7-amino-4-methylcoumarin (MetAMC) serves as a substrate for the *Escherichia coli* methionine aminopeptidase (MetAP) catalyzed reaction, and is routinely used for screening compounds to identify potential antibiotic agents. In pursuit of screening the enzyme's inhibitors, we observed that 2-hydroxypropyl-β-cyclodextrin (HP-β-CD), utilized to solubilize hydrophobic inhibitors, inhibited the catalytic activity of the enzyme, and such inhibition was not solely due to sequestration of the substrate by HP-β-CD.
Methods: The mechanistic path for the HP-β-CD mediated inhibition of MetAP was probed by performing a detailed account of steady-state kinetics, ligand binding, X-ray crystallographic, and molecular modeling studies.
Results: X-ray crystallographic data of the β-cyclodextrin–substrate (β-CD–MetAMC) complex reveal that while the AMC moiety of the substrate is confined within the CD cavity, the methionine moiety protrudes outward. The steady-state kinetic data for inhibition of MetAP by HP-β-CD–MetAMC conform to a model mechanism in which the substrate is "bridged" between HP-β-CD and the enzyme's active-site pocket, forming HP-β-CD–MetAMC–MetAP as the catalytically inactive ternary complex. Molecular modeling shows that the scissile bond of HP-β-CD-bound MetAMC substrate does not reach within the proximity of the enzyme's catalytic metal center, and thus the substrate fails to undergo cleavage.
Conclusions: The data presented herein suggests that the bridging of the substrate between the enzyme and HP-β-CD cavities is facilitated by interaction of their surfaces, and the resulting complex inhibits the enzyme activity.
General significance: Due to its potential interaction with physiological proteins via sequestered substrates, caution must be exercised in HP-β-CD mediated delivery of drugs under pathophysiological conditions.

1. Introduction

The ever increasing need for therapeutic controls has prompted an urgent drive toward identification of novel enzyme targets as well as new methods of inhibiting or modulating enzyme activities. Over the past decade, methionine aminopeptidases (MetAPs) have been identifed as potential targets for designing anticancer [1,2], antimicrobial [3,4] and anti-obesity agents [5]. Methionine aminopeptidase is responsible for the removal of N-terminal methionine from polypeptides during the process of translation. In about 80% of proteins, the universally present N-terminal methionine has to be removed from newly synthesized polypeptide in order for proper processing under physiological condition, and failure to do so results in non-functional or unstable proteins [6,7]. Mutational studies have shown that the MetAP gene is essential for survival in bacteria [8,9] and cell proliferation in eukaryotes [10–12]. In various reports, inhibitors of MetAPs have been identified as potential anticancer [1,13,14], antimalarial [15,16], antibacterial [17,18] and anti-obesity [19,20] drugs. Due to the fact that bacteria contain a single distinct class (Type I) of the enzyme as opposed to those present in eukaryotes (Types I and II), there has been interest in designing isozyme selective inhibitors against bacterial MetAP as desirable antibiotic agents.

While screening small molecular compounds, we identified several potent inhibitors of *E. coli* MetAP with binding affinities up to the nanomolar range [21]. However, due to poor solubility of some such compounds, we could not evaluate their potencies under *in vivo* conditions. To enhance the solubility of such inhibitors, we considered using cyclodextrins as the macromolecular carrier. In view of undertaking

Abbreviations: MetAP, methionine aminopeptidase; MetAMC, methionyl-7-amino-4-methylcoumarin; HP-β-CD, 2-hydroxypropyl-β-cyclodextrin

☆ The crystallographic coordinates of β-CD–MetAMC complex has been deposited at the Cambridge Crystallographic Data Center under the deposition number: CCDC 855352.

* Correspondence to: N. Sule, Department of Chemical Engineering, 3122 TAMU, College Station, TX 77843, United States. Tel.: +1 979 845 1433.
** Correspondence to: D.K. Srivastava, Department of Chemistry & Biochemistry, NDSU Dept 2735, PO Box 6050, Fargo, ND 58108, United States. Tel.: +1 701 231 7831; fax: +1 701 231 8324.
E-mail addresses: nitesh@tamu.edu (N.V. Sule), dk.srivastava@ndsu.edu (D.K. Srivastava).

http://dx.doi.org/10.1016/j.bbagen.2014.10.016
0304-4165/

such venture, we investigated the effect of cyclodextrins on the enzyme catalyzed reaction *in vitro*.

Cyclodextrins are constituted of cyclic rings contributed by 6, 7 or 8 glucopyranose units, referred to as α, β and γ cyclodextrins, respectively, and are shaped as toroids with a hydrophilic exterior surface and lipophilic core/cavity. They form inclusion complexes with a wide range of compounds and depending on the interacting guest moiety, their dissociation constants range over several orders of magnitude. Due to their non-polar cavity as well as low toxicity, cyclodextrins have been widely used as complexing and solubilizing agents in food, cosmetic and drug industries in addition to their applications as novel research tools [22–27]. They are known to enhance the bioavailability of drugs by facilitating their permeability (aside from solubility and stability) to cells under physiological conditions. Of the different cyclodextrins, 2-hydroxypropyl-β-cyclodextrin (referred herein as HP-β-CD) has been found to be the most effective drug carrier, and it has been successfully used in the formulation of poorly soluble drugs [28].

While attempting to use HP-β-CD to solubilize and stabilize some of our MetAP inhibitors [16], we realized that the above macromolecular carrier was drastically impairing the catalytic activity of the enzyme. This was initially conceived to be solely due to the sequestration of the enzyme's substrate (MetAMC) within the HP-β-CD's cavity, which would deplete the enzymatically utilizable aqueous form of the substrate, resulting in the inhibition of the enzyme. While this simplistic model has been established with other enzyme systems [29–31], we found that the HP-β-CD mediated inhibition of MetAP was predominantly due to the formation of the HP-β-CD–MetAMC–MetAP complex, and that the latter occurs via bridging of the substrate between the HP-β-CD and the enzyme's active site pocket. As will be elaborated in the Results section, while the AMC moiety of the substrate remained confined to the cavity/core of cyclodextrin, the methionine moiety interacted within the active site pocket of the enzyme. Since this assembly served as the dead-end complex, the overall catalytic efficiency of the enzyme was impaired. The experimental data leading to the above conclusion are discussed in the following sections.

2. Materials and methods

2.1. Materials

2-Hydroxypropyl-β-cyclodextrin and β-cyclodextrin were purchased from Sigma-Aldrich (St. Louis, MO). Methionyl-7-amino-4-methylcoumarin (MetAMC) was purchased from Enzo Life Sciences International Inc (Plymouth Meeting, PA). All other reagents were of analytical grade.

2.2. Expression and purification of MetAP

The recombinant form of *E. coli* MetAP (*Ec*MetAP) was expressed and purified as described previously [32]. The purity of MetAP was confirmed by the SDS-PAGE, and the protein concentration was determined by the Bradford method. The enzyme was stored at −70 °C in the presence of 30% glycerol in the storage buffer (25 mM HEPES, pH 7.5, containing 100 mM NaCl).

2.3. Enzyme activity

The catalytic activity of MetAP was determined using MetAMC as the fluorogenic substrate in a 96 well plate at room temperature, using a GeminiEM microplate reader (Molecular Devices, Sunnyvale, CA). In a typical assay system, 0.75 μM MetAP was added to the assay buffer (25 mM HEPES, pH 7.5, containing 100 mM NaCl, 10 μM $CoCl_2$) and the assay was initiated by addition of MetAMC. The reaction progress was monitored at 460 nm ($\lambda_{ex} = 360$ nm). The slope of the linear region of the reaction trace was taken as the measure of the initial rate of the enzyme catalyzed reaction. The slope was converted to concentration of product formed per unit time, using a standard curve (0.01–1 mM) of 7-amino-4-methylcoumarin (AMC) fluorescence obtained under the same conditions as the enzyme assay.

2.4. Spectrofluorometric studies

The spectral acquisition and spectrofluorometric titration studies for the binding of MetAMC to HP-β-CD were carried out on a Quantamaster spectrofluorometer (Photon Technology International, Birmingham, NJ). The HP-β-CD was titrated into 10 μM MetAMC in the above assay buffer and the fluorescence emission spectra were measured using a Xenon light source ($\lambda_{ex} = 315$ nm, $\lambda_{em} = 360$–540 nm). The signal to noise ratio was improved by using a 320 nm long-pass filter as well as by averaging 5 spectra. The increase in fluorescence intensity at 465 nm was plotted as a function of HP-β-CD concentration, and the data were analyzed by a complete solution of the quadratic function as described by Wang et al. [33] using Origin 7.0 software.

2.5. Kinetic studies for the inhibition of MetAP

The catalytic activity of MetAP was measured (as described above) at varying substrate concentrations (10–800 μM MetAMC). The K_m and k_{cat} parameters for the MetAP catalyzed reaction were obtained from the plot of the initial reaction velocity as a function of the substrate concentration, and the data were analyzed via Dynafit 3 software (BioKin Ltd., Watertown, MA) [34]. For inhibition studies, the enzyme activity was measured in the presence of varying concentrations of the substrate (10–800 μM) as well as HP-β-CD (0–12 mM). The steady-state kinetic data were analyzed for different types of inhibition models via the Dynafit software. The best model was identified based on the Akaike weight using the model discrimination analysis according to Burnham and Anderson [35].

2.6. Crystallization of the β-CD–MetAMC complex and determination of the structure

For crystallization of β-CD–MetAMC complex, 1 mmol solutions of β-cyclodextrin (β-CD) and MetAMC were prepared in water and ethanol, respectively. The solutions were slowly mixed and heated to 60 °C and maintained at the temperature for 2 h. This was followed by slowly cooling the reaction mixture which resulted in the formation of the β-CD–MetAMC crystals.

Single crystal X-ray diffraction data set was collected on a Bruker Apex Duo diffractometer (I μS microfocus Cu-radiation) with an Apex 2 CCD area detector. The structure was solved by direct methods and refined on *F*2 using Apex 2 v2010.9-1 software package, after integration with SAINT v7.68A and multi-scan absorption correction.

2.7. Molecular modeling studies

The docking studies of MetAMC to HP-β-CD and *Ec*MetAP were carried out using the software Autodock Vina 1.1.1 [36]. *Ec*MetAP crystal structure from PDB (2GTX) [37] was used as the model for the enzyme. β-CD crystal structure from the crystallized β-CD–MetAMC complex was used as the molecular model to build the structure for HP-β-CD. The docking input files were prepared using AutoDock Tools 1.5.6rc1 [38]. For docking the HP-β-CD–MetAMC complex to *Ec*MetAP, the grid box (28 × 28 × 26 Å) was centered over the enzyme active site and the exhaustiveness parameter for Vina was set at 50.

Molecular dynamics simulations were conducted with the all-atom CHARMM22 force field [39] in NAMD 2.8 [40] using VMD 1.9.1 [41] for the preparation of the input files. The topology and parameter files for HP-β-CD and MetAMC were generated using SWISS-PARAM [42]. In a typical setup the molecules were placed in a conformation close to that in the expected complex. The protein backbone was constrained, the molecules were solvated in a water sphere with a padding of 15 Å

using the TIP3P water model [43], and ions (Na^+ and Cl^-) were added at a concentration of 100 mM NaCl. The simulation was run with spherical boundary conditions at 300 K (with Langevin dynamics) for up to 150 ps, with 1 fs time steps. Non-bonded interactions were cut-off at 12 Å using a switching function at 10 Å and the bond-lengths and bond-angles of water molecules were constrained using the SHAKE algorithm [44]. The equilibration of the systems was confirmed by RMSD analysis and the interaction (nonbond) energies of the stabilized systems were calculated by NAMD.

3. Results

3.1. Effect of HP-β-CD on MetAP catalyzed reaction

In a preliminary manner, we noted that the MetAP catalyzed cleavage of the fluorogenic substrate (MetAMC) was inhibited in the presence HP-β-CD. To elucidate the molecular basis of the HP-β-CD mediated inhibition, we determined the time courses of the MetAP catalyzed reaction in the presence of 400 μM MetAMC substrate as a function of increasing concentration of HP-β-CD. Fig. 1 shows the linear increase in the fluorescence intensity ($\lambda_{ex} = 360$ nm, $\lambda_{em} = 460$ nm), due to the enzyme catalyzed cleavage of MetAMC to methionine and AMC, as a function of time. The slopes of such plots yielded the initial rates of the enzyme catalysis, which decreased with increase in the HP-β-CD concentration. As concluded by other investigators, we suspected that the presence of HP-β-CD depleted the free substrate (due to the formation of the HP-β-CD-substrate complex) leading to the impairment in the catalytic rate of the enzyme. Such expectation has been in accord with the literature precedent that CD inhibits catalysis of other enzymes by sequestering their substrates and thus reducing the concentration of free substrates in solution [29–31,45]. To probe whether or not the HP-β-CD mediated inhibition of MetAP was exclusively due to the sequestration/depletion of the enzyme's substrate; we proceeded to determine the binding affinity of MetAMC substrate with HP-β-CD as well as determine the kinetic parameters of the MetAP catalyzed reaction under an identical experimental condition. As shown below, these parameters allowed us to predict the rates of the MetAP catalyzed reaction (on the basis that the free substrate was the only substrate utilized during the enzyme catalysis) under diverse experimental conditions and compare them with those observed experimentally. To our surprise, under no condition did the predicted rate of the enzyme catalysis match with the experimentally observed rate. Such disparity between the observed and predicted rates prompted us to unravel the mechanism of the HP-β-CD mediated inhibition of the MetAP catalyzed reaction as elaborated below.

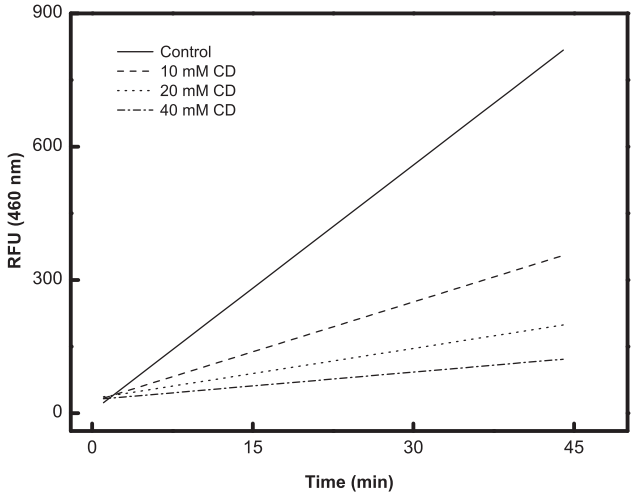

Fig. 1. Inhibition of MetAP by 2-hydroxypropyl-β-cyclodextrin (HP-β-CD). The catalytic activity of 1 μM MetAP was measured in a 96 well micro-titer plate in assay buffer (25 mM HEPES pH 7.5, 100 mM NaCl, 10 μM $CoCl_2$) with 400 μM of substrate (MetAMC) in the absence (Control) and presence of 10, 20 and 40 mM HP-β-CD, by monitoring the release of AMC ($\lambda_{ex} = 360$ nm, $\lambda_{em} = 460$ nm) over time using a plate reader.

3.2. Binding affinity of HP-β-CD–MetAMC complex

The spectral properties of fluorogenic guest molecules are known to be affected upon binding to the HP-β-CD cavity due to changes in their microenvironment [46]. To probe the influence of HP-β-CD on the fluorescence profile of MetAMC, we recorded the fluorescence emission spectra of 10 μM MetAMC ($\lambda_{ex} = 315$ nm) in the absence and presence of 20 mM HP-β-CD (Fig. 2). It should be pointed out that while the excitation maximum for MetAMC is 350 nm, we observed that by using the excitation wavelength of 315 nm along with a 320 nm long pass filter, the signal to noise ratio of the emission spectra in the 360–540 nm range was considerably improved. The data of Fig. 2 reveals that the presence of HP-β-CD decreased and increased the fluorescence emission intensity of MetAMC at 360 nm and 460 nm, respectively. Using this change in fluorescence emission intensity as a signal for the interaction of MetAMC with HP-β-CD, we could determine the binding affinity of the HP-β-CD–MetAMC complex by titrating a fixed concentration of MetAMC with increasing concentrations of HP-β-CD. The inset of Fig. 2 shows the HP-β-CD concentration dependent increase in the fluorescence emission intensity of MetAMC at 460 nm ($\lambda_{ex} = 315$ nm). The solid smooth line represents the best fit of the data for the dissociation constant (K_d) of the HP-β-CD–MetAMC complex as being equal to 3.50 ± 0.25 mM. A similar binding affinity (2.5 ± 0.4 mM) was obtained by monitoring the decrease in the fluorescence emission intensity of MetAMC at 360 nm (data not shown).

3.3. Steady-state kinetics of the MetAP catalyzed reaction

We determined the time courses for the MetAP catalyzed reaction by monitoring the increase in the fluorescence emission intensity at 460 nm ($\lambda_{ex} = 360$ nm) as a function of the substrate concentration. Fig. 3 shows the hyperbolic dependence of the enzyme catalyzed reaction rate as a function of MetAMC concentration. The solid smooth line is the best fit of the data according to the Michaelis-Menten equation with K_m and k_{cat} values of 76 ± 6 μM and 0.066 ± 0.002 min^{-1},

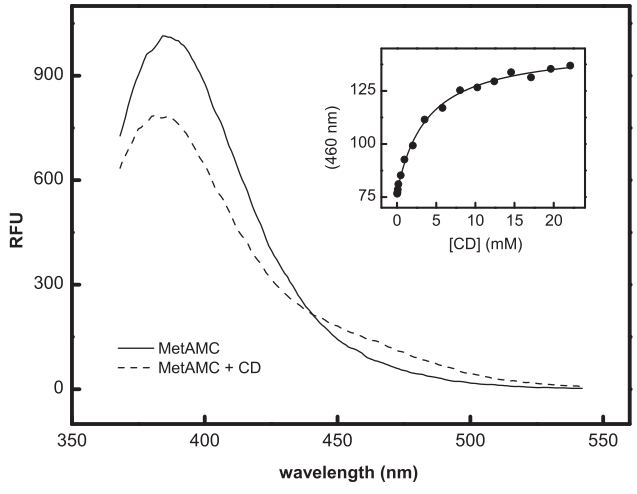

Fig. 2. Fluorescence properties of MetAMC in the absence and presence of HP-β-CD. The emission spectra of 10 μM MetAMC in the absence (solid) and presence (dashed) of 20 mM HP-β-CD were recorded in assay buffer ($\lambda_{ex} = 315$ nm). The inset shows the binding isotherm for the interaction of MetAMC with HP-β-CD. The increase in intensity at 460 nm on titration of HP-β-CD into 10 μM Met-AMC is plotted as a function of HP-β-CD concentration. The smooth line is the best fit of the data for the Kd value of the HP-β-CD–Met-AMC complex as being equal to 3.50 ± 0.25 mM.

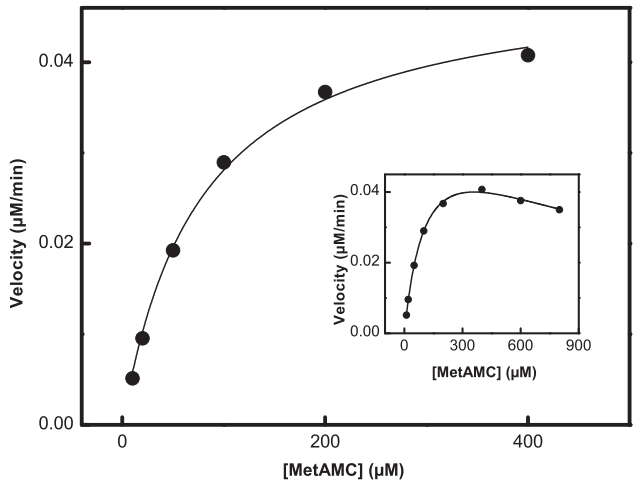

Fig. 3. Steady-state kinetics of the MetAP catalyzed cleavage of MetAMC substrate. The activity of 0.75 μM MetAP was assayed in a 96 well micro-titer plate. The reaction was initiated by the addition of varying concentrations of substrate (10–400 μM MetAMC) and monitored at 460 nm ($\lambda_{ex} = 360$ nm) using a plate reader. The slope of the linear portion of the reaction trace was used to calculate the initial velocity using AMC standard plot. The smooth line represents the best fit of the data for the values of K_m and k_{cat} as being equal to 76 ± 6 μM and 0.066 ± 0.002 s^{-1} respectively. The inset shows the enzyme catalyzed reaction velocity in the presence of extended range of substrate (10–800 μM MetAMC) concentration. The smooth line represents the best fit of the data according to Scheme 2 for the values of K_m, K_{mi} and k_{cat} being equal to 123 ± 9 μM, 1045 ± 121 μM and 0.090 ± 0.004 min^{-1}, respectively.

respectively. The above k_{cat} value was derived by converting the changes in the fluorescence intensity (during the course of the reaction) to the concentration unit using AMC as the standard (see Materials and methods).

In pursuit of determining K_m and k_{cat} values of MetAP catalyzed reaction using MetAMC as the substrate, we noted that the enzyme was undergoing inhibition at higher concentrations of the substrate. The inset of Fig. 3 shows the initial rate of the enzyme catalysis as a function of the extended range of the substrate concentration. Note that at high substrate concentration (>0.3 mM), the rate of the enzyme catalysis decreases. Such a decrease in activity has often been attributed to the inner filter effect in fluorogenic assays [47]. However, it was experimentally confirmed that the increase in fluorescence signal of the substrate remained linear even at high concentrations (up to 1 mM) under assay conditions. Therefore the decreased activity at higher substrate concentrations could not be ascribed to the inner filter effect. On the other hand, this inhibition feature has been observed with several other enzymes [48] and its origin has been frequently ascribed to the formation of ES_2 complex, which is catalytically non-productive as depicted in Scheme 1.

In Scheme 1, E and S represent MetAP (enzyme) and MetAMC (substrate). On assumption that the formation of ES and ES_2 complexes is under rapid equilibrium, the initial rate of the MetAP catalyzed reaction can be given by Eq. (1):

$$V = \frac{V_{max} \times S}{K_m + S\left(1 + \frac{S}{K_{mi}}\right)} \quad (1)$$

where K_m and K_{mi} refer to the dissociation constants of ES and ES_2 complexes, respectively. The solid smooth line is the best fit of the data for K_m, K_{mi} and k_{cat} values of 123 ± 9 μM, 1045 ± 121 μM and 0.090 ± 0.004 min^{-1}, respectively. Note that the latter value is similar to the k_{cat} derived at lower concentration of the substrate (the condition under which there was no substrate inhibition). A comparison between the K_m and K_{mi} values suggests that the binding of the second substrate to the ES complex is about 8 fold weaker than the binding of substrate to the free enzyme.

3.4. Elucidation of the kinetic mechanism of the HP-β-CD mediated inhibition of MetAP

Given the derived thermodynamic and kinetic parameters from the data of Figs. 2 and 3, respectively, we could predict the rate of the MetAP catalyzed reaction as a function of the HP-β-CD concentration on the assumption that the free substrate (MetAMC) was the only substrate utilized during the enzyme catalysis. The above assumption slightly modifies the kinetic Scheme 1 in the form of Scheme 2. Note that Scheme 2 incorporates an additional equilibration step, i.e., the binding of MetAMC with HP-β-CD. The binding affinity (K_d value) of the HP-β-CD–MetAMC complex was derived from the data of Fig. 2. The predicted rate for this scheme could be calculated using a modified form of Eq. (1) by substituting $S = K_d \times [SCD]/[CD]$, where K_d is 3.5 mM (Fig. 2) and [SCD] is given by the quadratic solution of the binding function [33].

To test the validity of the model of Scheme 2, we determined the rate of the MetAP catalyzed reaction as a function of HP-β-CD concentration in the presence of 0.8 mM concentration of MetAMC (the concentration where substrate inhibition becomes pronounced) and compared the experimental data (solid circles; Fig. 4) with those predicted (solid line) on the assumption that the free substrate was the only substrate utilized during the course of the enzyme catalysis. Note a marked disparity between the experimental and predicted data of Fig. 4A, suggesting that the model mechanism of Scheme 2 is inadequate to explain our

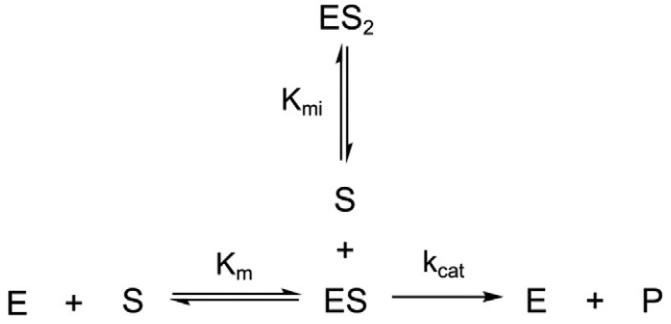

Scheme 1. Model mechanism of the MetAP catalyzed cleavage of MetAMC, incorporating substrate inhibition.

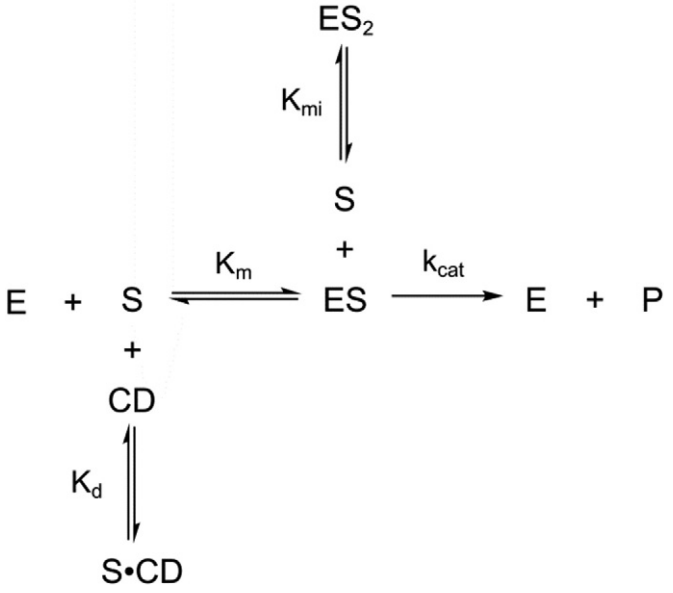

Scheme 2. Expected mechanism for inhibition of the MetAP catalyzed reaction due to sequestration of the substrate by cyclodextrin.

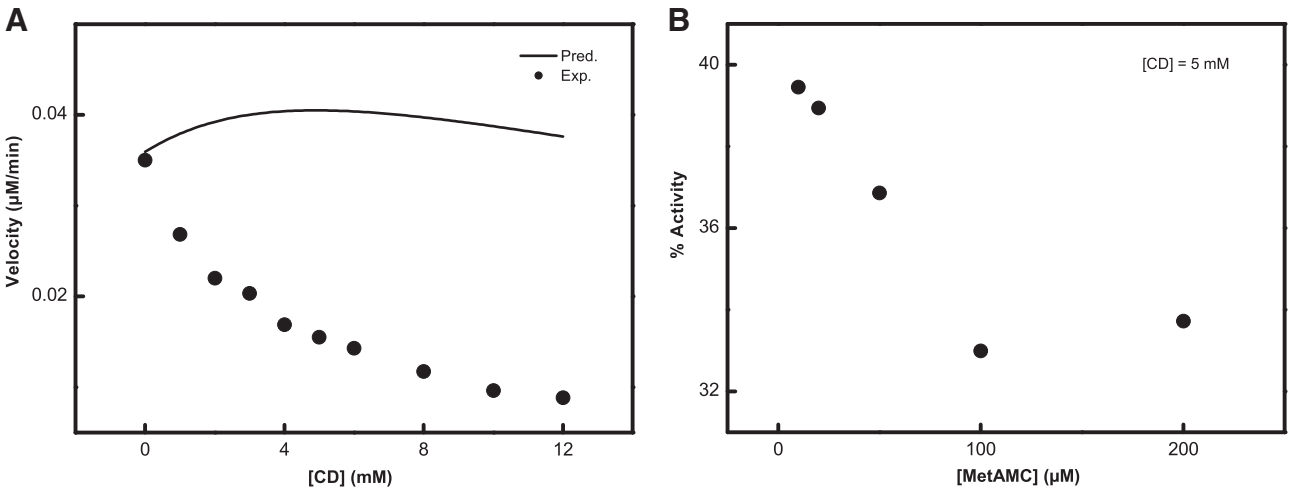

Fig. 4. (A). Experimentally observed versus predicted rates of the MetAP catalyzed reaction. The solid dots are the observed reaction velocities for MetAP catalyzed reaction with varying CD concentrations in the presence of 800 μM substrate (MetAMC). The solid smooth line represents the calculated reaction velocities as per the "competitive" inhibition model of Scheme 2, using the experimentally determined parameters of K_m, k_{cat} and K_d. (B) Effect of substrate concentration on inhibition of MetAP by CD. The enzyme activity in the presence of 5 mM HP-β-CD is plotted as a percentage of the activity in the absence of HP-β-CD, at varying concentrations of substrate. The decreasing profile indicates that increasing concentrations of substrate results in an enhanced inhibitory effect of the HP-β-CD.

experimental results. The lack of conformity of the model of Scheme 2 was further substantiated by the experimental observation that the enzyme catalysis in the presence of HP-β-CD was more inhibited at higher concentrations of the substrate than at lower concentrations (Fig. 4B). These observations led to the hypothesis that HP-β-CD–MetAMC complex was serving as an inhibitor of the MetAP catalyzed reaction. To further elaborate on this feature, we determined the rates of the MetAP catalyzed reactions as a function of varying concentrations of MetAMC and HP-β-CD as shown in Fig. 5. Whereas Fig. 5A shows the substrate (MetAMC) dependence of the enzyme catalysis at changing fixed concentrations of HP-β-CD, Fig. 5B shows the HP-β-CD concentration dependent inhibition of the enzyme catalysis at changing fixed concentrations of the substrate.

A casual perusal of the data of Fig. 5 revealed the following features: (i) the substrate inhibition is most pronounced in the absence of HP-β-CD; as the HP-β-CD concentration increases, the substrate inhibition becomes progressively weaker; (ii) the plateau of the individual plots (representative of the maximum velocity values) for the enzyme catalysis progressively decreases with increase in the HP-β-CD concentration; and (iii) the apparent K_m for the substrate progressively decreases with increase in the HP-β-CD concentration. These observations led to the suggestion that besides binding to the free substrate, HP-β-CD also interacts with the ES complex, and the latter binding is likely to be facilitated due to bridging of MetAMC between HP-β-CD and MetAP within the HP-β-CD–MetAMC–MetAP complex. As shown below, this feature is supported by our X-ray crystallographic data of the CD–MetAMC complex in conjunction with the modeling studies for the interaction of HP-β-CD–MetAMC with MetAP.

In view of the above experimental outcomes, it appeared evident that the kinetic mechanism for the inhibition of MetAP by HP-β-CD was formalistically similar to the mixed type of inhibition, except for the fact that unlike classical mixed-type of inhibition, HP-β-CD (the inhibitor) interacted with the substrate instead of with the enzyme (Scheme 3).

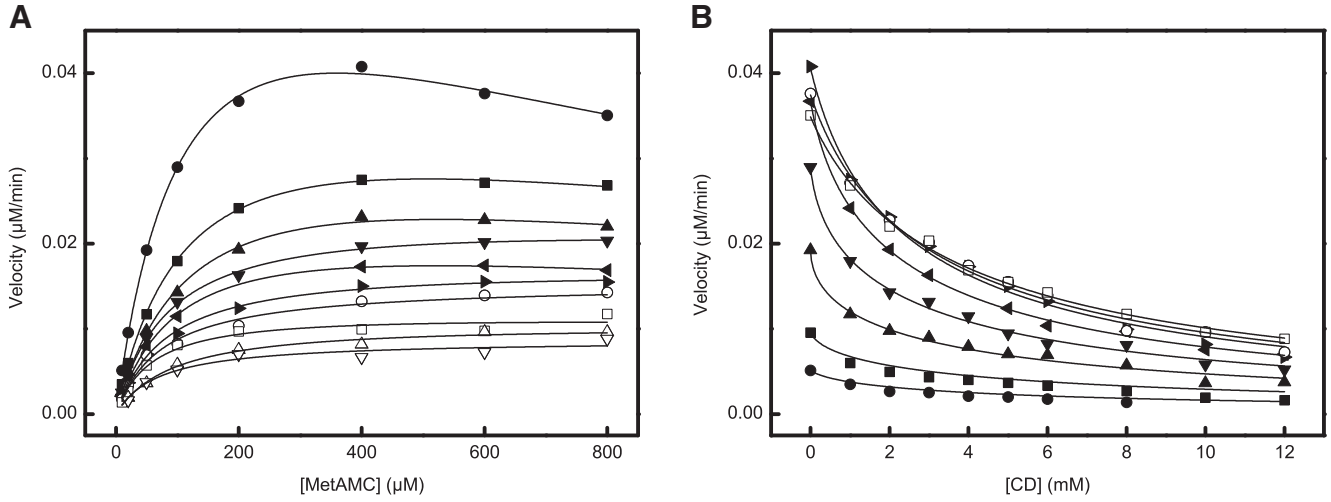

Fig. 5. Inhibition of the MetAP catalyzed reaction as a function HP-β-CD at different concentrations of the (MetAMC) substrate. The activity of 0.75 μM MetAP was measured in a 96 well micro-titer plate in assay buffer (25 mM HEPES pH 7.5, 100 mM NaCl, 10 μM $CoCl_2$) with 10–1000 μM substrate (MetAMC) in the presence of 0–12 mM HP-β-CD. (A) The rates of the enzyme catalyzed reaction as a function of substrate (MetAMC) concentration in the presence of 0 (●), 1 (■), 2 (▲), 3 (▼), 4 (◄), 5 (►), 6 (○), 8 (□), 10 (Δ) and 12 (▽) mM HP-β-CD. (B) Replot of the data of (A) as a function of HP-β-CD concentration at 10 (●), 20 (■), 50 (▲), 100 (▼), 200 (◄), 400 (►), 600 (○) and 800 (□) μM substrate (MetAMC). The smooth lines represent the best fit of the data using the model depicted in Scheme 3, for the values of K_m, k_{cat}, K_{mi}, K_m', K_d and K_d' being equal to 143 ± 17 μM, 0.090 ± 0.006 min^{-1}, 894 ± 148 μM, 55 ± 5 μM, 3.3 ± 0.4 mM and 1.2 ± 0.1 mM, respectively.

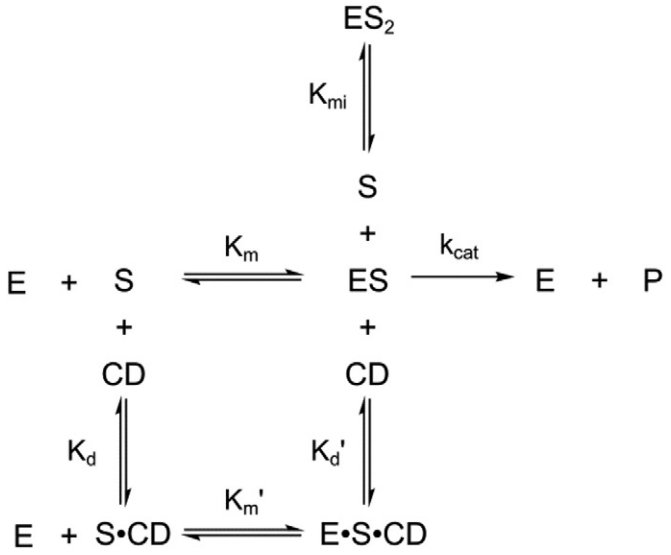

Scheme 3. Model mechanism satisfying the catalytic and binding affinity data from Figs. 2, 3 and 5.

Although Scheme 3 appeared to be most plausible minimal model for analyzing the comprehensive data of Fig. 5, we could not rule out other plausible mechanisms with subtle variations in the above scheme. Such variations involved (among others): (i) HP-β-CD–MetAMC complex not being converted to HP-β-CD–MetAMC–MetAP complex as found in the case of the CD dependent inhibition of polyphenol oxidases as well as other enzymes [45,49], (ii) HP-β-CD–MetAMC–MetAP serving as the productive complex, (iii) interaction of HP-β-CD with free enzyme (followed by formation of HP-β-CD–MetAMC–MetAP complex). To analyze the data of Fig. 5 by the model of Scheme 3 vis a vis its variants, we employed Dynafit software. Besides performing the non-linear regression analysis by simply providing the kinetic model in a script format (rather than final form of the derived equation), the above software is ideally suited for distinguishing between various alternative kinetic mechanisms by using the Akaike information criterion (AIC), whereby the most plausible model is identifiable by the highest Akaike weight and the relative significance of the models is given by delta AIC (Δ_i) such that $\Delta_i < 2$ suggests substantial evidence for the model, values between 3 and 7 indicate that the model has considerably less support and $\Delta_i > 10$ indicates that the model is very unlikely (*25*). When we analyzed the data of Fig. 5, the best fit of the data adhered to the minimal model mechanism of Scheme 3. The solid smooth lines are the best fit of the experimental data with K_m, k_{cat}, K_{mi}, K_m', K_d and K_d' as being equal to 143 ± 17 μM, 0.090 ± 0.006 min^{-1}, 894 ± 148 μM, 55 ± 5 μM, 3.3 ± 0.4 mM and 1.2 ± 0.1 mM respectively. Note that the values of K_m, k_{cat}, K_{mi} and K_d are similar to those determined from independent experiments (Figs. 2 and 3). It should be emphasized that no other kinetic mechanism produced an even approximate fit to our data. According to the model discrimination analysis, whereas the Akaike weight of the model described in Scheme 3 was ≈1 (with $\Delta_i < 2$), that of all other models was ≈0 (with Δ_i ranging $5 < \Delta_i < 120$). It should be pointed out that apparent binding affinity of HP-β-CD for free substrate is lower (K_d = 3.3 mM) than that for the enzyme bound substrate (K_d' = 1.2 mM), suggesting that there is a finite contribution of the enzyme's surface in enhancing the binding affinity of the substrate for HP-β-CD. We therefore specifically considered additional pathways to mechanism in Scheme 3, for example, HP-β-CD interacting with free enzyme forming HP-β-CD–MetAP complex, followed by binding of the substrate to form the ternary complex. Although such mechanisms were disqualified as highly improbable through model discrimination analysis in Dynafit, it did not completely rule out their possibility since the Akaike information criterion penalizes models for each additional step. However as shown below, this probable additional pathway is rejected by our modeling data lending further support to Scheme 3.

3.5. X-ray crystallographic structure of β-CD–MetAMC complex

To ascertain the mode of binding of MetAMC to HP-β-CD, we proceeded to crystallize these compounds for X-ray crystallographic studies. However, we soon realized that 2-hydroxypropyl-β-cyclodextrin (HP-β-CD), utilized during all experiments reported herein, was difficult to crystallize. Thus, we resorted to using β-CD (without the hydroxypropyl groups) and crystallized it in complex with MetAMC as described in the Experimental section. The crystallization protocol yielded diffraction quality colorless plate-like crystals after two weeks, whose structure was solved. Details of the data collection and refinement are given in Supplementary Table S1. Fig. 6 shows the X-ray crystallographic structure of β-CD–MetAMC complex. The structural data reveals that while the coumarin moiety of MetAMC is buried within the cyclodextrin cavity, the methionine residue is exposed to the exterior solvent environment. The length of the exposed residue from the tip of the methionine side chain to the peptide carbonyl oxygen is 6.5 Å. Since β-CD was used instead of HP-β-CD for crystallization of the cyclodextrin–substrate complex, we examined the effect of β-CD on the MetAP assay and found that it was a poor inhibitor as compared to the 2-hydroxypropyl derivatized CD (data not shown). However, the global structure of the β-CD–MetAMC complex is unlikely to be different from that of the HP-β-CD–MetAMC complex; therefore the structural data of former complex was taken as the representative of the latter, and was used for rationalizing our kinetic and molecular modeling results (see below). An alternative approach would have been to validate the structure of HP-β-CD–MetAMC complex by NMR spectroscopy [50,51], but we could not perform such experiment.

3.6. Molecular modeling studies for the formation of HP-β-CD–MetAMC–MetAP complex

In order to provide the molecular basis for the HP-β-CD dependent inhibition of MetAP catalyzed reaction in view of our steady-state

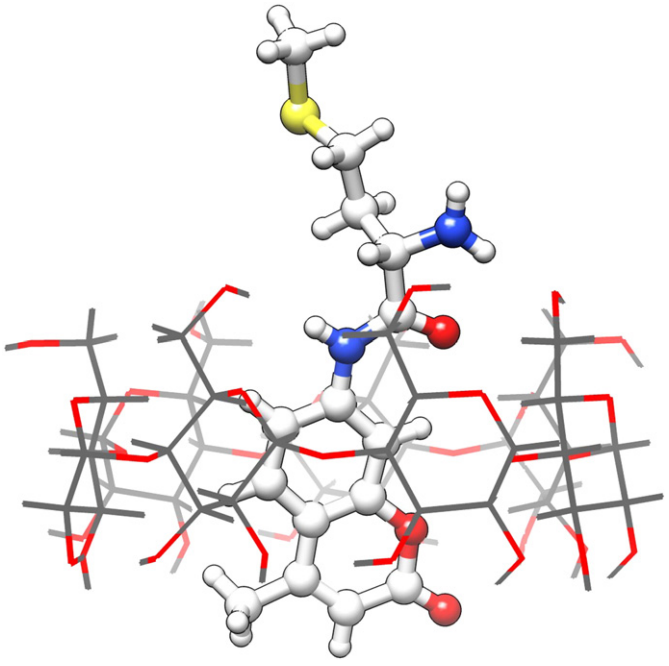

Fig. 6. The X-ray crystallographic structure of the β-CD–MetAMC complex. The structures of β-CD and MetAMC are represented by wire and ball and stick models respectively. Note that the methionine residue of MetAMC is protruding out of the β-CD cavity.

kinetic data (Scheme 3, Fig. 5), as well as the X-ray crystallographic structure of the β-CD–MetAMC complex (Fig. 6), we performed molecular modeling studies by docking the HP-β-CD–MetAMC complex with the known structural coordinates of MetAP using Autodock Vina (ver 1.1.1) software (as described in the Experimental section). Fig. 7 shows the docked structure of HP-β-CD–MetAMC complex (HP-β-CD, blue; MetAMC, green ball and stick) with MetAP (gray). The inset clipped view reveals the interaction of the methionine residue of the free substrate (magenta stick) with the active site pocket of the enzyme (gray). As indicated earlier, the methionine residue projects 6.5 Å out from the HP-β-CD cavity and it is long enough to enter into the active site pocket within the HP-β-CD–MetAMC–MetAP complex. However within the above complex, the scissile bond of MetAMC does not reach in the vicinity of the active site resident metal ion, and thus the enzyme catalyzed cleavage of the bridged MetAMC (between HP-β-CD and MetAP) is precluded, resulting in the inhibition of the enzyme catalyzed reaction as per the model mechanism of Scheme 3.

In order to further substantiate or refute the model for the formation of the ternary complex as described in Scheme 3 as well as to test the viability of alternative pathways of formation of the HP-β-CD–MetAMC–MetAP complex, we performed MD simulations of the system in the following configurations: (i) substrate (MetAMC) placed near the cyclodextrin cavity (S + CD), (ii) substrate placed near the enzyme active-site pocket (E + S), (iii) substrate placed between the enzyme active-site pocket and the cyclodextrin cavity (E + S + CD), and (iv) cyclodextrin placed between the enzyme active site pocket and the substrate (E + CD + S) (see supplementary data). Fig. 8 shows the RMSD of the substrate for each of the above simulations. Note that the substrate molecule moved an average of 4 Å to achieve the most energetically stable conformation in the S + CD, E + S and E + S + CD simulations (by occupying the cavity of cyclodextrin, enzyme or both, respectively). On the other hand the position of substrate molecule remained relatively unchanged (rmsd ≈ 1) in the case of E + CD + S signifying that the ternary complex could not be formed by the prior interaction of cyclodextrin with free enzyme, followed by binding of substrate. The interaction energy of the substrate within the enzyme active site pocket (in the MetAP–MetAMC or ES complex) was calculated to be −330 kcal/mol. Whereas the interaction energy of the methionine residue alone in the active-site pocket in the HP-β-CD–MetAMC–MetAP complex was calculated to be −259 kcal/mol, the total interaction energy of the ternary complex was slightly lower than that of the ES complex (−340 kcal/mol). This appeared to be due to the contributions of the interactions between substrate and cyclodextrin (−42 kcal/mol) and between enzyme and cyclodextrin (−39 kcal/mol), thus providing the drive for the formation of the stable ternary complex. On the other hand, the total interaction energy in the case of the E + CD + S simulation (where free E first binds to free CD, followed by binding of S) was only −111 kcal/mol, which is significantly greater than the above complexes indicating insufficient energetic rationale for the formation of the HP-β-CD–MetAMC–MetAP complex via this mechanism and validating the exclusion of this pathway in the proposed model of Scheme 3. The modeling data suggests that the molecular surfaces may be involved in enhancing the interaction with MetAP in the HP-β-CD–MetAMC–MetAP complex.

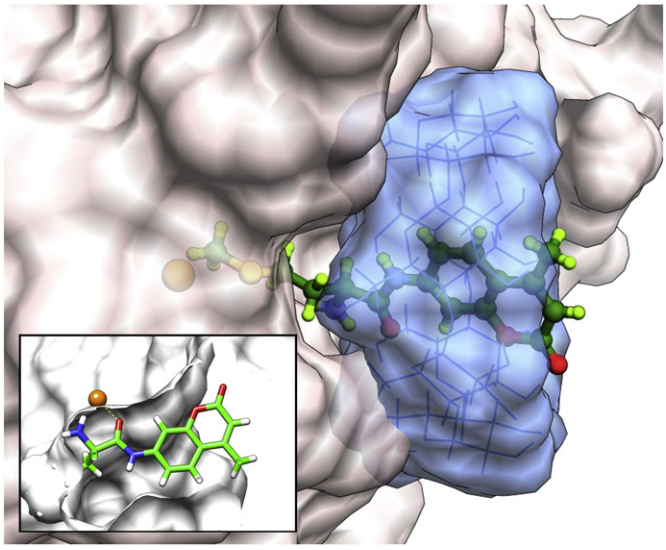

Fig. 7. MD simulation of the binding of HP-β-CD–MetAMC complex with MetAP. The structural coordinates of β-CD–MetAMC (Fig. 6) were docked to the active site pocket of MetAP. Note that in the docked structure, the methionine residue of MetAMC (green) extends into (and interacts with) the enzyme's active site pocket (gray) while the coumarin moiety of the substrate remains confined into the cavity of β-CD cavity (blue). The distance between the metal ion and the peptidyl oxygen in the docked structure was found to be 10 Å away from the active site resident metal ion. The inset shows the structure of the free substrate MetAMC (magenta) docked at the enzyme's active site (gray). In this case, the distance between the peptidyl oxygen and metal ion is 2.8 Å. Clearly, the cleavable peptidyl bond of the β-CD confined MetAMC does not extend deep into the active site pocket of the enzyme to undergo the cleavage reaction, and thus the resultant complex inhibits the enzyme activity.

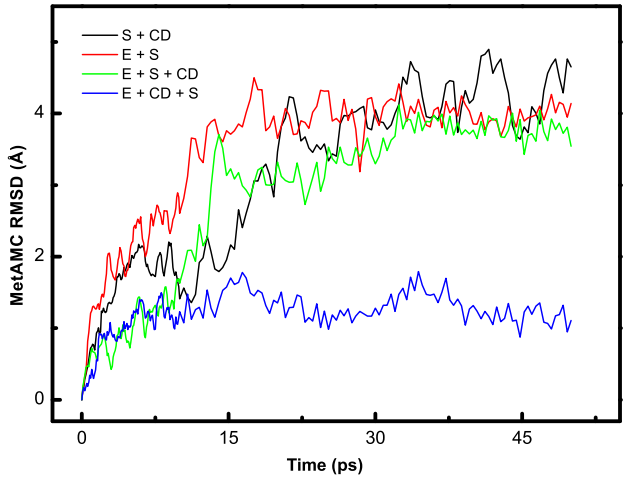

Fig. 8. RMSD of MetAMC after MD simulations with enzyme and cyclodextrin. The molecules in each system were positioned to mimic the pathway of complex formation described in Scheme 3 (except for E + CD + S which is not described in the scheme). The large value of RMSD of MetAMC for the S + CD, E + S and E + S + CD simulations (~4 Å) indicate the translocation of the substrate to within the cavity of the cyclodextrin, enzyme active-site or both, resulting in the formation of the respective complexes. The low RMSD for the E + CD + S simulation (~1 Å) indicates that the substrate remained in solution and the ternary complex did not form.

4. Discussion

The experimental data presented in this paper provide a unique mechanism for the inhibition of MetAP by HP-β-CD, and to the best of our knowledge, no such mechanistic feature has been previously demonstrated for any enzyme. We provide evidence for the first time that the HP-β-CD mediated inhibition of MetAP is not exclusively due to the sequestration of the enzyme's substrate by HP-β-CD, but it is also due to the formation of HP-β-CD–MetAMC–MetAP as the non-productive ("dead-end") ternary complex. The latter is manifested via bridging of the two ends of the substrate structure, viz., AMC and methionine moieties, between HP-β-CD and MetAP, respectively.

Cyclodextrins have been known to affect the activity of many enzymes via different mechanisms. They have been found to enhance the activity of enzymes by solubilizing poorly soluble substrates [39], complexing with inhibitors [31,52] or by stabilizing the enzymes under adverse conditions [53,54]. On the other hand, CDs have been known to inhibit the enzyme activities primarily via reduction of the free substrate concentrations due to their sequestration within the

cavity [29–31]. Similar to the observation of Rodríguez-Bonilla et al. [55] we also found that the inhibition of the enzyme at high substrate concentrations was relieved upon addition of HP-β-CD presumably due to sequestration of the substrate. In our effort to delineate the mechanistic pathway for the inhibition of MetAP catalyzed reaction (using MetAMC as substrate) in the presence of HP-β-CD, we came to the conclusion that the mere sequestration of the enzyme's substrate by HP-β-CD is not the exclusive mechanism for inhibiting MetAP (and possibly other enzymes). This could be easily conceived by comparing the experimental rates of enzyme catalysis in the presence of HP-β-CD versus those predicted on the basis of reduction in the free substrate concentration due to sequestration by HP-β-CD (Fig. 4A). There are some reports on the non-competitive or mixed inhibition of selected enzymes by cyclodextrins which have been attributed to an unknown mode of cyclodextrin-enzyme interaction in addition to the observed sequestration of substrate [30,45,56,57]. To our surprise (and contrary to the reports of the reversal of inhibition of the enzyme activity by CD in the presence of increasing concentrations of substrate; [58]), we observed that increase in the substrate (MetAMC) concentration enhanced the magnitude of inhibition of the enzyme by HP-β-CD (Fig. 4B). As elaborated in the Results section, the latter feature has been due to the added inhibition (i.e., aside from the sequestration of the substrate) of the enzyme caused by the formation of the non-productive (dead-end) ternary complex involving bridged substrate between HP-β-CD and MetAP. Our analysis of the substrate and HP-β-CD concentration dependent enzyme catalyzed reaction data (Fig. 5) by alternative kinetic models unequivocally supported the model mechanism of Scheme 3.

Although we could not provide independent physical evidence for the direct interaction of HP-β-CD–MetAMC complex with MetAP (due to their relatively weak binding affinity), a combination of the X-ray crystallographic structure of the β-CD–MetAMC complex coupled with the molecular modeling studies lead to support the prevalence of such complex during the kinetic course of the HP-β-CD dependent inhibition of the enzyme catalyzed reaction. In view of the crystallographic structure of the β-CD–MetAMC complex, it appeared evident that the protruded methionine residue (while AMC being confined within the cyclodextrin cavity) would not be able to completely reach into the active site pocket of the enzyme. The molecular modeling data suggests that the scissile amide bond of the substrate would fall short (by about 7 Å) from reaching the metal ion at the catalytic center of the enzyme. Assuming that the above void would be occupied by two water molecules such that they are bridged between the active site resident metal ion and the thioether group of the methionine residue, the latter would be stabilized within the enzyme's active site pocket both via hydrophobic interaction as well as the water mediated hydrogen bonding. However, since the HP-β-CD bound MetAMC does not serve as direct substrate during the enzyme catalysis, it was surmised that the binding energy of the substrate within the both enzyme and HP-β-CD cavities (in the ternary complex) is either greater than or equal to the binding energy of the substrate within the enzyme's active site pocket in the ES complex alone. This was corroborated by the interaction energies obtained through the MD simulations of the complexes. The total interaction energy of the HP-β-CD–MetAMC–MetAP complex is lower than the total sum of the interaction energies of each binary complex (HP-β-CD–MetAMC, MetAMC–MetAP and HP-β-CD–MetAP) alone. Evidently, these individual binding energies are modulated by the overall energetics of the unique interaction between the molecular surfaces involved in the formation of the HP-β-CD–MetAMC–MetAP ternary complex, resulting in the stable complex and the observed inhibitory profile.

The generality or frequency of such mechanism in other enzyme systems must await further studies particularly since there is an emerging trend of using HP-β-CD as the macromolecular carriers for enzyme inhibitors in the drug discovery endeavor. However, the use of HP-β-CD as the drug carrier may have undesirable consequences under the physiological system. In fact, underivatized α-, β- and γ-cyclodextrins are known to have cytotoxic and nephrotoxic effects [59]. Hence, in view of our mechanistic studies, it is possible that free CDs in drug formulations (either pre-existing, or following the release of the drugs), may interact with other substrates/ligands and the cyclodextrin–ligand complexes can interact with cognate enzymes/proteins resulting in the inhibition of unintended targets. In view of these possibilities, caution must be exercised before employing cyclodextrins as the general/routine drug carriers.

Funding

This work was supported by the NIH grants CA113746 and CA132034 to DKS and SM.

Acknowledgments

Molecular graphics images were produced using the UCSF Chimera package [60] from the Resource for Biocomputing, Visualization, and Informatics at the University of California, San Francisco (supported by NIH P41 RR001081). MD simulations were run using NAMD developed by the Theoretical and Computational Biophysics Group in the Beckman Institute for Advanced Science and Technology at the University of Illinois at Urbana-Champaign.

Appendix A. Supplementary data

Supplementary data to this article can be found online at http://dx.doi.org/10.1016/j.bbagen.2014.10.016.

References

[1] E.C. Griffith, Z. Su, B.E. Turk, S. Chen, Y.H. Chang, Z. Wu, K. Biemann, J.O. Liu, Methionine aminopeptidase (type 2) is the common target for angiogenesis inhibitors AGM-1470 and ovalicin, Chem. Biol. 4 (1997) 461–471.
[2] H. Endo, K. Takenaga, T. Kanno, H. Satoh, S. Mori, Methionine aminopeptidase 2 is a new target for the metastasis-associated protein, S100A4, J. Biol. Chem. 277 (2002) 26396–26402.
[3] W.T. Lowther, Y. Zhang, P.B. Sampson, J.F. Honek, B.W. Matthews, Insights into the mechanism of *Escherichia coli* methionine aminopeptidase from the structural analysis of reaction products and phosphorus-based transition-state analogues, Biochemistry (Mosc) 38 (1999) 14810–14819.
[4] L. Chen, J. Li, J.-Y. Li, Q.-L. Luo, W.-F. Mao, Q. Shen, F.-J. Nan, Q.-Z. Ye, Type I methionine aminopeptidase from *Saccharomyces cerevisiae* is a potential target for antifungal drug screening, Acta Pharmacol. Sin. 25 (2004) 907–914.
[5] A.A. Joharapurkar, N.A. Dhanesha, M.R. Jain, Inhibition of the methionine aminopeptidase 2 enzyme for the treatment of obesity, Diabetol. Metab. Syndr. Obes. Targets Ther. 7 (2014) 73–84.
[6] S.M. Arfin, R.L. Kendall, L. Hall, L.H. Weaver, A.E. Stewart, B.W. Matthews, R.A. Bradshaw, Eukaryotic methionyl aminopeptidases: two classes of cobalt-dependent enzymes, Proc. Natl. Acad. Sci. U. S. A. 92 (1995) 7714–7718.
[7] T. Meinnel, Y. Mechulam, S. Blanquet, Methionine as translation start signal: a review of the enzymes of the pathway in Escherichia coli, Biochimie 75 (1993) 1061–1075.
[8] S.Y. Chang, E.C. McGary, S. Chang, Methionine aminopeptidase gene of *Escherichia coli* is essential for cell growth, J. Bacteriol. 171 (1989) 4071–4072.
[9] C.G. Miller, A.M. Kukral, J.L. Miller, N.R. Movva, pepM is an essential gene in *Salmonella typhimurium*, J. Bacteriol. 171 (1989) 5215–5217.
[10] X. Li, Y.H. Chang, Amino-terminal protein processing in *Saccharomyces cerevisiae* is an essential function that requires two distinct methionine aminopeptidases, Proc. Natl. Acad. Sci. U. S. A. 92 (1995) 12357–12361.
[11] M. Boxem, C.W. Tsai, Y. Zhang, R.M. Saito, J.O. Liu, The *C elegans* methionine aminopeptidase 2 analog map-2 is required for germ cell proliferation, FEBS Lett. 576 (2004) 245–250.
[12] S.G. Bernier, N. Taghizadeh, C.D. Thompson, W.F. Westlin, G. Hannig, Methionine aminopeptidases type I and type II are essential to control cell proliferation, J. Cell. Biochem. 95 (2005) 1191–1203.
[13] A.C. Cooper, R.M. Karp, E.J. Clark, N.R. Taghizadeh, J.G. Hoyt, M.T. Labenski, M.J. Murray, G. Hannig, W.F. Westlin, C.D. Thompson, A novel methionine aminopeptidase-2 inhibitor, PPI-2458, inhibits Non–Hodgkin's lymphoma cell proliferation in vitro and in vivo, Clin. Cancer Res. 12 (2006) 2583–2590.
[14] J. Lu, C.R. Chong, X. Hu, J.O. Liu, Fumarranol, a rearranged fumagillin analogue that inhibits angiogenesis in vivo, J. Med. Chem. 49 (2006) 5645–5648.
[15] X. Chen, C.R. Chong, L. Shi, T. Yoshimoto, D.J. Sullivan, J.O. Liu, Inhibitors of *Plasmodium falciparum* methionine aminopeptidase 1b possess antimalarial activity, Proc. Natl. Acad. Sci. 103 (2006) 14548–14553.
[16] P. Zhang, D.E. Nicholson, J.M. Bujnicki, X. Su, J.J. Brendle, M. Ferdig, D.E. Kyle, W.K. Milhous, P.K. Chiang, Angiogenesis inhibitors specific for methionine aminopeptidase 2 as drugs for Malaria and Leishmaniasis, J. Biomed. Sci. 9 (2002) 34–40.

[17] S. Bhat, O. Olaleye, K.J. Meyer, W. Shi, Y. Zhang, J.O. Liu, Analogs of N′-hydroxy-N-(4H,5H-naphtho[1,2-d]thiazol-2-yl)methanimidamide inhibit *Mycobacterium tuberculosis* methionine aminopeptidases, Bioorg. Med. Chem. 20 (2012) 4507–4513.
[18] P. Wangtrakuldee, M.S. Byrd, C.G. Campos, M.W. Henderson, Z. Zhang, M. Clare, A. Masoudi, P.J. Myler, J.R. Horn, P.A. Cotter, T.J. Hagen, Discovery of inhibitors of *Burkholderia pseudomallei* methionine aminopeptidase with antibacterial activity, ACS Med. Chem. Lett. 4 (2013) 699–703.
[19] Y.M. Kim, J.J. An, Y.-J. Jin, Y. Rhee, B.S. Cha, H.C. Lee, S.-K. Lim, Assessment of the anti-obesity effects of the TNP-470 analog, CKD-732, J. Mol. Endocrinol. 38 (2007) 455–465.
[20] T.E. Hughes, D.D. Kim, J. Marjason, J. Proietto, J.P. Whitehead, J.E. Vath, Ascending dose-controlled trial of beloranib, a novel obesity treatment for safety, tolerability, and weight loss in obese women, Obesity (Silver Spring) 21 (2013) 1782–1788.
[21] M.K. Haldar, M.D. Scott, N. Sule, D.K. Srivastava, S. Mallik, Synthesis of barbiturate-based methionine aminopeptidase-1 inhibitors, Bioorg. Med. Chem. Lett. 18 (2008) 2373–2376.
[22] E.M.M. Del Valle, Cyclodextrins and their uses: a review, Process Biochem. 39 (2004) 1033–1046.
[23] S.V. Kurkov, T. Loftsson, Cyclodextrins, Int. J. Pharm. 453 (2013) 167–180.
[24] L. García-Río, F.J. Otero-Espinar, A. Luzardo-Alvarez, J. Blanco-Méndez, Cyclodextrin based rotaxanes, polyrotaxanes and polypseudorotaxanes and their biomedical applications, Curr. Top. Med. Chem. 14 (2014) 478–493.
[25] J.M. López-Nicolás, P. Rodríguez-Bonilla, F. García-Carmona, Cyclodextrins and antioxidants, Crit. Rev. Food Sci. Nutr. 54 (2014) 251–276.
[26] A.A. Elbashir, N.F.A. Dsugi, T.O.M. Mohmed, H.Y. Aboul-Enein, Spectrofluorometric analytical applications of cyclodextrins, Lumin. J. Biol. Chem. Lumin. 29 (2014) 1–7.
[27] L. Escuder-Gilabert, Y. Martín-Biosca, M.J. Medina-Hernández, S. Sagrado, Cyclodextrins in capillary electrophoresis: recent developments and new trends, J. Chromatogr. A 1357 (2014) 2–23.
[28] R. Challa, A. Ahuja, J. Ali, R.K. Khar, Cyclodextrins in drug delivery: an updated review, AAPS PharmSciTech 6 (2005) E329–E357.
[29] P.L. Irwin, P.E. Pfeffer, L.W. Doner, G.M. Sapers, J.D. Brewster, G. Nagahashi, K.B. Hicks, Binding geometry, stoichiometry, and thermodynamics of cyclomalto-oligosaccharide (cyclodextrin) inclusion complex formation with chlorogenic acid, the major substrate of apple polyphenol oxidase, Carbohydr. Res. 256 (1994) 13–27.
[30] E. Núñez-Delicado, M. Mar Sojo, A. Sánchez-Ferrer, F. García-Carmona, Hydroperoxidase activity of lipoxygenase in the presence of cyclodextrins, Arch. Biochem. Biophys. 367 (1999) 274–280.
[31] E. Orenes-Piñero, F. García-Carmona, A. Sánchez-Ferrer, Kinetic characterization of diphenolase activity from *Streptomyces antibioticus* tyrosinase in the presence and absence of cyclodextrins, J. Mol. Catal. B Enzym. 47 (2007) 143–148.
[32] N. Sule, R.K. Singh, P. Zhao, D.K. Srivastava, Probing the metal ion selectivity in methionine aminopeptidase via changes in the luminescence properties of the enzyme bound europium ion, J. Inorg. Biochem. 106 (2012) 84–89.
[33] Z.-X. Wang, N. Ravi Kumar, D.K. Srivastava, A novel spectroscopic titration method for determining the dissociation constant and stoichiometry of protein–ligand complex, Anal. Biochem. 206 (1992) 376–381.
[34] P. Kuzmic, Program DYNAFIT for the analysis of enzyme kinetic data: application to HIV proteinase, Anal. Biochem. 237 (1996) 260–273.
[35] K.P. Burnham, D.R. Anderson, Model Selection and Multimodel Inference: A Practical Information-Theoretic Approach, 2nd ed. Springer, New York, 2002.
[36] O. Trott, A.J. Olson, AutoDock Vina: improving the speed and accuracy of docking with a new scoring function, efficient optimization, and multithreading, J. Comput. Chem. 31 (2010) 455–461.
[37] Q.-Z. Ye, S.-X. Xie, Z.-Q. Ma, M. Huang, R.P. Hanzlik, Structural basis of catalysis by monometalated methionine aminopeptidase, Proc. Natl. Acad. Sci. U. S. A. 103 (2006) 9470–9475.
[38] M.F. Sanner, Python: a programming language for software integration and development, J. Mol. Graph. Model. 17 (1999) 57–61.
[39] A.D. MacKerell, D. Bashford, M. Bellott, R.L. Dunbrack, J.D. Evanseck, M.J. Field, S. Fischer, J. Gao, H. Guo, S. Ha, D. Joseph-McCarthy, L. Kuchnir, K. Kuczera, F.T.K. Lau, C. Mattos, S. Michnick, T. Ngo, D.T. Nguyen, B. Prodhom, W.E. Reiher, et al., All-atom empirical potential for molecular modeling and dynamics studies of proteins, J. Phys. Chem. B 102 (1998) 3586–3616.
[40] J.C. Phillips, R. Braun, W. Wang, J. Gumbart, E. Tajkhorshid, E. Villa, C. Chipot, R.D. Skeel, L. Kalé, K. Schulten, Scalable molecular dynamics with NAMD, J. Comput. Chem. 26 (2005) 1781–1802.
[41] W. Humphrey, A. Dalke, K. Schulten, VMD: visual molecular dynamics, J. Mol. Graph. 14 (1996) 33–38.
[42] V. Zoete, M.A. Cuendet, A. Grosdidier, O. Michielin, SwissParam: a fast force field generation tool for small organic molecules, J. Comput. Chem. 32 (2011) 2359–2368.
[43] W.L. Jorgensen, J. Chandrasekhar, J.D. Madura, R.W. Impey, M.L. Klein, Comparison of simple potential functions for simulating liquid water, J. Chem. Phys. 79 (1983) 926–935.
[44] J.-P. Ryckaert, G. Ciccotti, H.J. Berendsen, Numerical integration of the cartesian equations of motion of a system with constraints: molecular dynamics of n-alkanes, J. Comput. Phys. 23 (1977) 327–341.
[45] A. Koralewska, W. Augustyniak, A. Temeriusz, M. Kańska, Effects of cyclodextrin derivatives on the catalytic activity of tyrosine phenol-lyase, J. Incl. Phenom. Macrocycl. Chem. 49 (2004) 193–197.
[46] A. Orstan, J.B.A. Ross, Investigation of the beta-cyclodextrin-indole inclusion complex by absorption and fluorescence spectroscopies, J. Phys. Chem. 91 (1987) 2739–2745.
[47] M.O. Palmier, S.R. Van Doren, Rapid determination of enzyme kinetics from fluorescence: overcoming the inner filter effect, Anal. Biochem. 371 (2007) 43–51.
[48] M.C. Reed, A. Lieb, H.F. Nijhout, The biological significance of substrate inhibition: a mechanism with diverse functions, BioEssays News Rev. Mol. Cell. Dev. Biol. 32 (2010) 422–429.
[49] S. Jingru, X. Yong, L. Zhuolin, Inhibition of α-hydroxybutyrate dehydrogenase activity by β-cyclodextrin derivatives, Am. Biotechnol. Lab 27 (2009) 27–30.
[50] Y. Yao, Y. Xie, C. Hong, G. Li, H. Shen, G. Ji, Development of a myricetin/hydroxypropyl-β-cyclodextrin inclusion complex: preparation, characterization, and evaluation, Carbohydr. Polym. 110 (2014) 329–337.
[51] C. Yuan, Z. Jin, X. Xu, Inclusion complex of astaxanthin with hydroxypropyl-β-cyclodextrin: UV, FTIR, 1H NMR and molecular modeling studies, Carbohydr. Polym. 89 (2012) 492–496.
[52] J.M. López-Nicolás, A.J. Pérez-López, Á. Carbonell-Barrachina, F. García-Carmona, Kinetic study of the activation of banana juice enzymatic browning by the addition of maltosyl-β-cyclodextrin, J. Agric. Food Chem. 55 (2007) 9655–9662.
[53] Â.M.L. Denadai, M.M. Santoro, M.T.P. Lopes, A. Chenna, F.B. de Sousa, G.M. Avelar, M.R. Túlio Gomes, F. Guzman, C.E. Salas, R.D. Sinisterra, A supramolecular complex between proteinases and β-cyclodextrin that preserves enzymatic activity: physicochemical characterization, BioDrugs 20 (2006) 283–291.
[54] E. Fasoli, B. Castillo, A. Santos, E. Silva, A. Ferrer, E. Rosario, K. Griebenow, F. Secundo, G.L. Barletta, Activation of subtilisin Carlsberg in organic solvents by methyl-β-cyclodextrin: lyoprotection versus substrate and product-complex effect, J. Mol. Catal. B Enzym. 42 (2006) 20–26.
[55] P. Rodríguez-Bonilla, L. Méndez-Cazorla, J.M. López-Nicolás, F. García-Carmona, Kinetic mechanism and product characterization of the enzymatic peroxidation of pterostilbene as model of the detoxification process of stilbene-type phytoalexins, Phytochemistry 72 (2011) 100–108.
[56] T. Gubica, E. Winnicka, A. Temeriusz, M. Kańska, The influence of selected O-alkyl derivatives of cyclodextrins on the enzymatic decomposition of l-tryptophan by l-tryptophan indole-lyase, Carbohydr. Res. 344 (2009) 304–310.
[57] T. Gubica, A. Pełka, K. Pałka, A. Temeriusz, M. Kańska, The influence of cyclomaltooligosaccharides (cyclodextrins) on the enzymatic decomposition of l-phenylalanine catalyzed by phenylalanine ammonia-lyase, Carbohydr. Res. 346 (2011) 1855–1859.
[58] E. Alvarez-Parrilla, L.A. de la Rosa, J. Rodrigo-García, R. Escobedo-González, G. Mercado-Mercado, E. Moyers-Montoya, A. Vázquez-Flores, G.A. González-Aguilar, Dual effect of β-cyclodextrin (β-CD) on the inhibition of apple polyphenol oxidase by 4-hexylresorcinol (HR) and methyl jasmonate (MJ), Food Chem. 101 (2007) 1346–1356.
[59] T. Irie, K. Uekama, Pharmaceutical applications of cyclodextrins. III. Toxicological issues and safety evaluation, J. Pharm. Sci. 86 (1997) 147–162.
[60] E.F. Pettersen, T.D. Goddard, C.C. Huang, G.S. Couch, D.M. Greenblatt, E.C. Meng, T.E. Ferrin, UCSF Chimera—a visualization system for exploratory research and analysis, J. Comput. Chem. 25 (2004) 1605–1612.